Design and Performance of an Ultra-Compact Low-Speed Low-Turbulence level Wind Tunnel for Aerodynamic and Animal Flight Experiments

Kenneth Breuer*
School of Engineering, Brown University, Providence RI 02912 USA

Mark Drela†
Dept. of Aeronautics and Astronautics, MIT, Cambridge MA 02139 USA

Xiaozhou Fan‡ and Matteo Di Luca§
School of Engineering, Brown University, Providence RI 02912 USA

The paper presents a novel closed-circuit ultra-compact wind tunnel with an 8:1 contraction ratio and high flow quality. Its key design features include a 2D-type main diffuser, a minimum-length contraction, and a screened expanding vane cascade in the last corner. These features reduce the overall tunnel footprint area to less than half of the area of a conventional tunnel design with the same test section size and same contraction ratio. The test section turbulence level is a very low 0.03% over a 4Hz–8500Hz bandwidth.

I. Nomenclature

C_p	pressure coefficient	U	speed in test section
K	screen pressure–loss coefficient	V	local speed
s	arc length along wall	x	coordinate along tunnel
u	speed fluctuation	y, z	transverse-plane coordinates

II. Introduction

Low-speed wind tunnels with low levels of freestream turbulence are desirable testing facilities in both academic and industrial laboratories for pursuing a wide variety of experimental goals. The majority of tests in such facilities are for engineering and physical science applications including testing of vehicle and wing configurations as well as fundamental fluid mechanics. For these applications, models are tested over extended periods of time and used for detailed experiments that might include measurements of surface pressure and/or flow field measurements using Pitot, hot-wire or Particle Image Velocimetry (PIV). In a "low-speed" facility, defined (somewhat arbitrarily) as one where the Mach number less than ~ 0.2 so that the flow can be considered incompressible, testing velocities can range over the range ~ 5–$50\,\mathrm{m/s}$.

A more unusual application that has seen increased interest in the past few years is that of animal flight testing; for such biological flight experiments, birds or bats are trained to fly in the tunnel while a variety of tests including, for example kinematic (e.g. wing motion) and velocity field (e.g. wake measurements), are conducted. For such applications, testing velocities tend to be lower than in aerodynamic testing (most animals fly at at velocities below 15–20 m/s), but apart from this constraint, the facility requirements for animal flight share many of the same goals as for engineering testing, including good flow uniformity, low turbulence levels, optical access to the test section and good control of temperature over a wide range of flow speeds and over a long testing duration.

The design of low-speed, low-turbulence wind tunnels has evolved over the past century, but has always involved tradeoffs between flow quality (uniformity and turbulence levels) against power consumption, construction costs, and size. An extensive review is given by Bradshaw and Pankhurst[1]. Larger contraction ratios are desirable to achieve low

*Professor, AIAA Associate Fellow
†Terry J. Kohler Professor, AIAA Fellow
‡Graduate Research Assistant
§Graduate Research Assistant

turbulence levels, but a large contraction ratio requires extensive expansion of the flow from the test section, through the fan and back to the settling chamber, screens and contraction. Achieving such expansion without boundary layer separation in the diffusers usually requires shallow expansion angles, and this leads to long flow paths and consequently a large facility footprint. A common approach to reduce the facility size has been the use of a wide-angle final diffuser, in which separation is prevented by the use of some number of screens or perforated plates, at the cost of somewhat greater power consumption and possibly a greater turbulence level compared to a conventional diffuser. More recently, innovations by Lindgren et al. which allow reduction of the overall tunnel size are vertically-expanding 2D diffusers[2], and expanding (diffusing) corner vanes[3]. This approach also reduces design complexity and construction costs due to the increased use of rectangular flow elements. A further development is the screened expanding vane concept of Drela et al.[4] in which separation in a cascade with the very large expansion ratio of 2:1 is suppressed by means of a screen placed at the exit of each vane passage. This concept was successfully demonstrated in both scale experiments and numerical simulations, but has not been yet applied in practice.

In this manuscript we describe a new wind tunnel facility at Brown University that is designed for both animal flight and engineering aeromechanics applications, As such it needs to exhibit good flow quality over a wide speed range and have a testing section that is suitable for a diverse series of experiments. These include measurements of aerodynamic forces on fixed models, flow field measurements using hot-wire anemometers and laser-based diagnostics such as PIV, and measurements of the kinematics and dynamics of birds and bats in free flight.

The wind tunnel design presented here incorporates, for the first time, all of the following recent design innovations: vertically-expanding second and main diffusers, a weakly expanding vane in corner 2 before the fan, and a strongly expanding screened vane in corner 4 before the flow-conditioning screens and contraction. Corner 4 also incorporates the honeycomb into its vane assembly, thus eliminating the length it would add to the screen section. Lastly the design also features a minimum-length contraction leading into the test section. All these features are aimed at giving the smallest possible tunnel footprint for the required test section size and contraction ratio. The paper will give an overview of the design philosophy and design techniques used for the tunnel components, and present the measurements of the flow quality in the test section.

III. Design considerations

A. Overall layout and design

As is often the case with wind tunnel design, two main factors that drove the present design were the tension between (i) the available space to locate the facility and (ii) the desired contraction ratio and test section dimensions. The current tunnel is housed entirely in an existing building, which limited the overall tunnel length to 51 feet. The maximum test section size is then constrained by the desired contraction ratio, and also by the length required by the diffusers to expand to the necessary settling chamber dimensions without risk of flow separation.

For the present tunnel, flowpath design iterations traded between the flow quality requirements and the space constraints, guided by quasi-1D integral boundary layer calculations to gauge the flow separation margins. 3D RANS calculations of the entire final flowpath were performed as a design verification.

The final tunnel layout is shown in figure 1. Corners 1 and 3 are conventional (non-expanding), Corner 2 expands slightly, and Corner 4 expands very aggressively which is enabled by the screened vanes. The main diffuser is two-dimensional and expands only vertically. A minimum-length contraction is also used. These design features give an ultra-compact tunnel which has only about 40% of the footprint area, and hence also lower construction costs, than an equivalent conventional-design tunnel with the same test section size. The specific design considerations for each component of the tunnel are discussed next.

B. Fan section

A fiberglass/epoxy transition section is used to change from a square to round cross section for the axial fan. The same section shape, in reverse, is used to convert back to a square section downstream of the fan. The annular flow area between the fan case and the motor nacelle is nearly the same as the square area immediately upstream and downstream of the fan.

The airflow is driven using a nine-bladed axial fan (Twin City) powered by a 125 HP AC motor (TECO) and a variable frequency drive (ABB ACH550). The fan blade angles can be manually adjusted to suit the desired operating characteristics. Since this facility is intended to operate extensively at low speeds, the blade angles were set at an

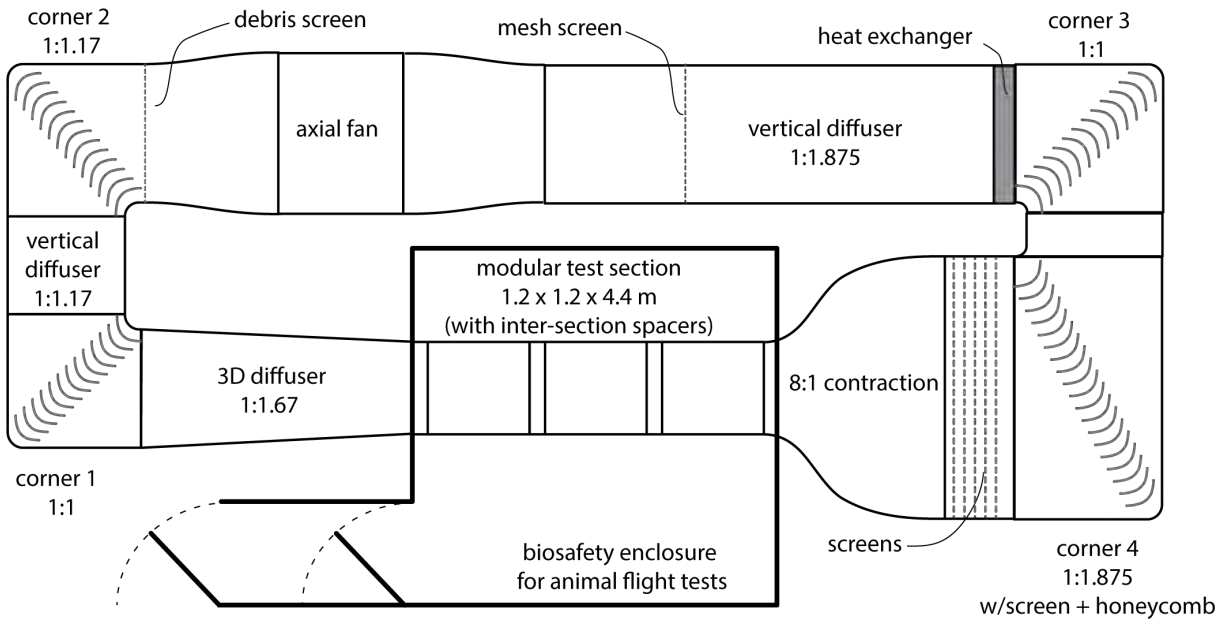

Fig. 1 Wind tunnel layout, viewed from above. The flow direction is clockwise. The overall tunnel footprint is 15.8 by 6.3 meters. The main diffuser at top expands only vertically, which is not visible in this view. The strongly expanding Corner 4 is in the lower right.

intermediate angle which reduces the maximum achievable speed in the tunnel but, by increasing the fan RPM at a given freestream velocity, provides a more stable flow at low speeds, suitable for animal flight experiments.

C. Diffusers

For the flowpath portion immediately after the test section, a length reduction shrinks the tunnel footprint, while width reduction does not. Therefore, a conventional three-dimensional design was used here for this first diffuser, with an area ratio of 1.67:1 and a wall half-angle of 3°. This relatively "safe" combination compensates for the thicker than usual boundary layers created by the relatively long test section.

In contrast to the first diffuser, both a small length and a small width are at a premium in the return leg of the tunnel. Hence, for the main diffuser after the fan a two-dimensional design was chosen, with a constant width and a vertical expansion. The area ratio is 1.875:1 and the wall expansion half-angle is 7.7°, which is a very aggressive combination. Hence, a wire-mesh screen is added about one-third down the expansion to suppress flow separation. The heat exchanger located at the diffuser end also acts as a second diffuser screen to suppress flow separation there.

D. Corner Vanes

The 12.7in chord turning vanes in Corner 1 have a pitch/chord ratio of 0.65, and are designed using the viscous/inviscid MISES cascade code[5] to operate without significant separation over the entire tunnel operating speed range, as shown in figure 2. The lowest tunnel speed causes the most difficulty with laminar separation, so to address this the vane is shaped to have a weak adverse pressure gradient over most of the suction surface. This intentionally destabilizes the boundary layer and thus encourages it to undergo transition at chord Reynolds numbers down to 38 000 (3000/inch) without laminar separation bubble bursting. The unavoidable penalty is some loss of laminar flow at the highest speeds. The pressure surface is designed for mostly laminar flow, and to meet manufacturing constraints. The vanes are extruded aluminum, which requires a minimum thickness of roughly 0.15in at the trailing edge. At maximum tunnel speed the predicted loss coefficient is 0.022, which is 20% more than what's possible (0.018) for an aerodynamically-ideal vane with a sharp trailing edge. This extra loss is, however, small in real terms, consuming only 0.06% of the tunnel drive power.

The Corner 2 vanes are physically the same as in Corner 1, but are staggered and angled differently to expand the flow area by the ratio 1.17:1 while giving the necessary 90° turning. The pitch/chord ratio is also reduced to 0.60, which

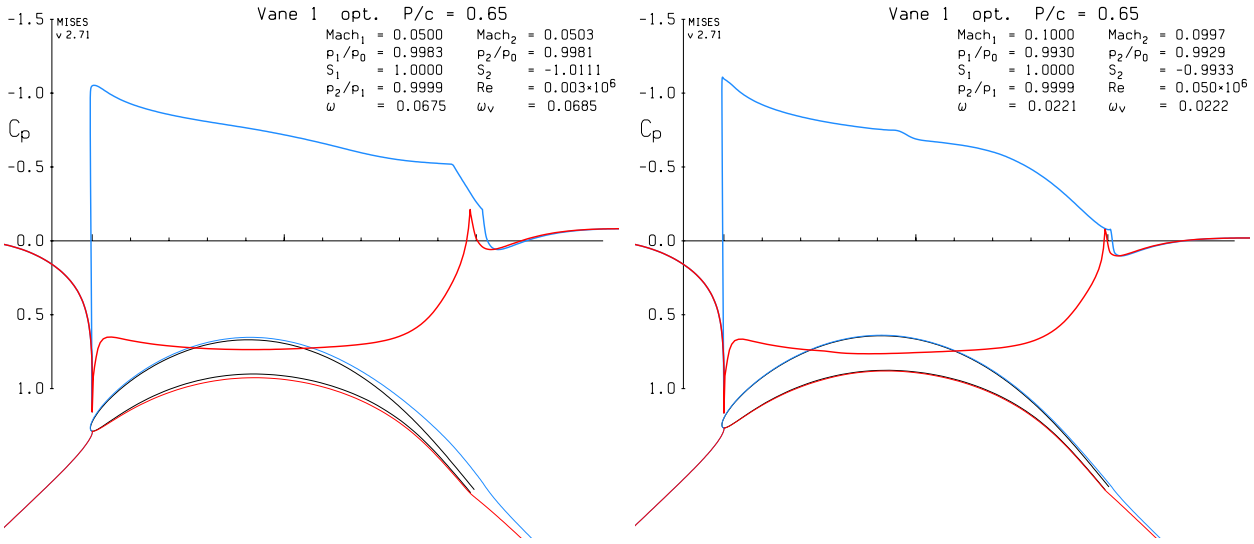

Fig. 2 Optimized Corner 1 vane with computed displacement surfaces and C_p distributions from MISES, for min (left) and max (right) tunnel speeds.

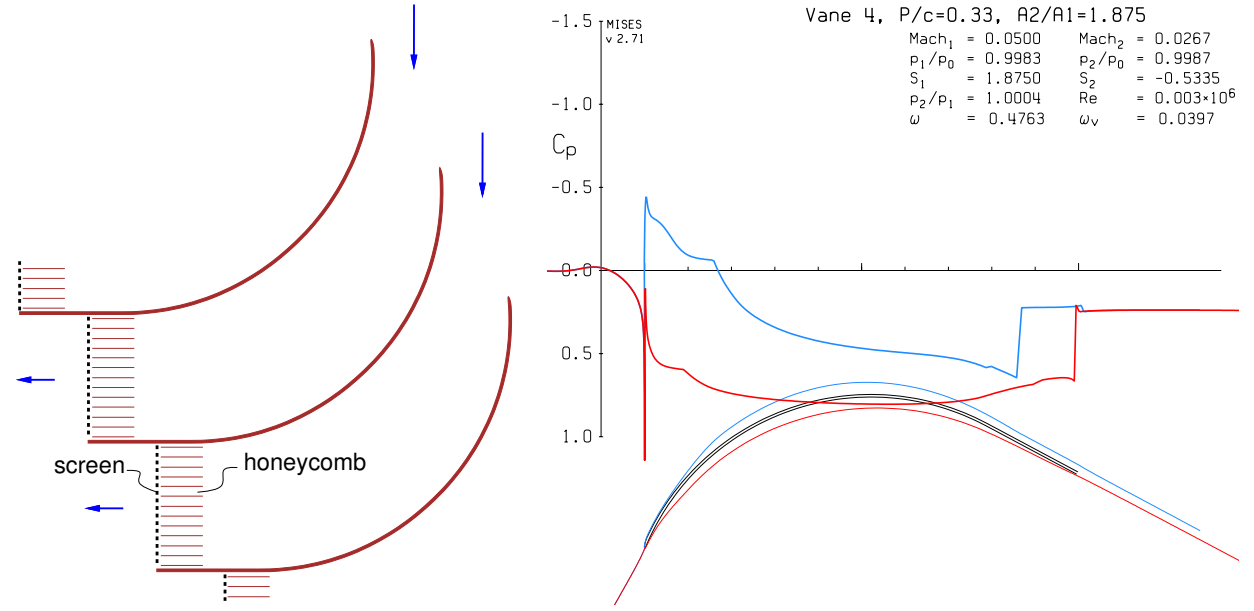

Fig. 3 Screened expanding turning vane cascade of corner 4, with flow area ratio of 1.875:1. MISES C_p distributions show screen pressure drop. The displacement-body surfaces along the vane show the boundary layer thinning effect of the screen within the flow passage.

compensates for the area expansion and prevents flow separation, at least according to the 2D MISES simulations. A debris screen positioned at the exit of Corner 2, immediately upstream of the fan section, helpfully acts to suppress any possible 3D separation from the Corner 2 vane/wall intersections from going into the fan.

Corner 3 vanes are a conventional non-expanding type, with a constant thickness. Based on MISES simulations, their designed shape is a simple 94° circular-arc with a straight trailing edge extension, and a pitch/chord of 0.40. The constant thickness and simple shape were chosen to be compatible with inexpensive rolled sheet steel construction. Their additional loss compared to the alternative fully optimized shape vanes is less than 0.005% of total drive power, which is an acceptably small penalty given their considerable construction cost savings.

Corner 4 features the screened expanding turning vane[4], which is the most innovative aspect of the tunnel design, and is the one which enables most of the tunnel footprint reduction. The specific vane design used here has a very aggressive expansion ratio of 1.875:1, and a pitch/chord ratio of 0.33. A constant thickness and a simple arc plus trailing edge extension shape are also used here for low cost. This vane concept has wire screening installed over each vane-passage exit to suppress flow separation which would otherwise occur inside each passage, as diagrammed in figure 3. Honeycomb is also installed immediately upstream of the screen, and suppresses any streamwise vorticity which might be produced in the vane passages. There is one honeycomb piece in each vane passage and between splitter plates, and this has the screen attached to it prior to installation (fig 4). The combined honeycomb+screen sections are installed in the vanes much like filter elements, and if necessary they can be replaced just as easily. This modular system avoids the high cost and structural-support difficulties of the typical large single-piece honeycomb used in conventional tunnels. In effect, Corner 4 combines the functions of a turning vane, a wide-angle diffuser, and a honeycomb, all with a near-zero added streamwise flow length.

Fig. 4 Section of screened vane, viewed from downstream.

E. Contraction

The design goal for the 8:1 contraction is to obtain the shortest possible distance between the last screen and the start of the test section without any laminar flow separation. A traditional high-order polynomial definition was found to have inadequate design freedom for this task, so roughly 50 x, r (streamwise-radial) coordinate pairs, interpolated by a cubic spline, define the wall shape. Initial axisymmetric design was performed by iterating geometric construction and inverse calculations with specified wall $C_p(s)$, using the viscous/inviscid MTFLOW code which is an axisymmetric version of MISES.

The contraction starts at the last screen but very slowly at first, so that the initial wall curvatures are small and the resulting adverse pressure gradients are kept below the laminar separation threshold. The slow initial contraction then makes the large end of the contraction function as a settling chamber, and it also minimizes the potential-flow distortion over the screen face, which in turn minimizes the total-pressure distortions leaving the screen. As the centerline favorable gradient gradually overcomes the wall adverse gradient, the contraction rate is progressively increased up to the maximum contraction rate of $\mathrm{d}r/\mathrm{d}x = -1.25$ at the inflection point. This is limited mainly by the suction peak and resulting adverse pressure gradient which appears on the convex wall just ahead of the test section entry. The final contraction length/width ratio is only 0.67:1, significantly shorter than the 1:1 ratio of conventional tunnels.

The initial axisymmetric channel design was converted to the necessary square cross-section channel, and fillets were also added, such that the flow area distribution was preserved. The resulting 3D wall shapes and the fillet widths were then fine-tuned using the QUAPDAN panel code[6], together with quasi-1D integral boundary layer calculations to check for separation. Figure 5 shows the surface speed contours from QUADPAN on one quadrant of the final contraction design. The fillets serve to weaken the superposition of the 2D wall pressure gradients at the corners, which avoids laminar separation and secondary flow development which would otherwise occur there. To maximize their benefit the fillets are "flared" such that they are widest near the contraction inflection, and taper upstream to a point at the last screen and also taper partially downstream into the test section. The flaring reduces the maximum surface speed on each fillet to only 1.09 times the test-section velocity, compared to 1.14 which would occur on a constant-width, or straight, fillet. The maximum surface speed ratio on the midlines is 1.05, shown in figure 6. The adverse pressure gradients past these modest overspeeds are very easily handled by the very thin turbulent boundary layers at those locations.

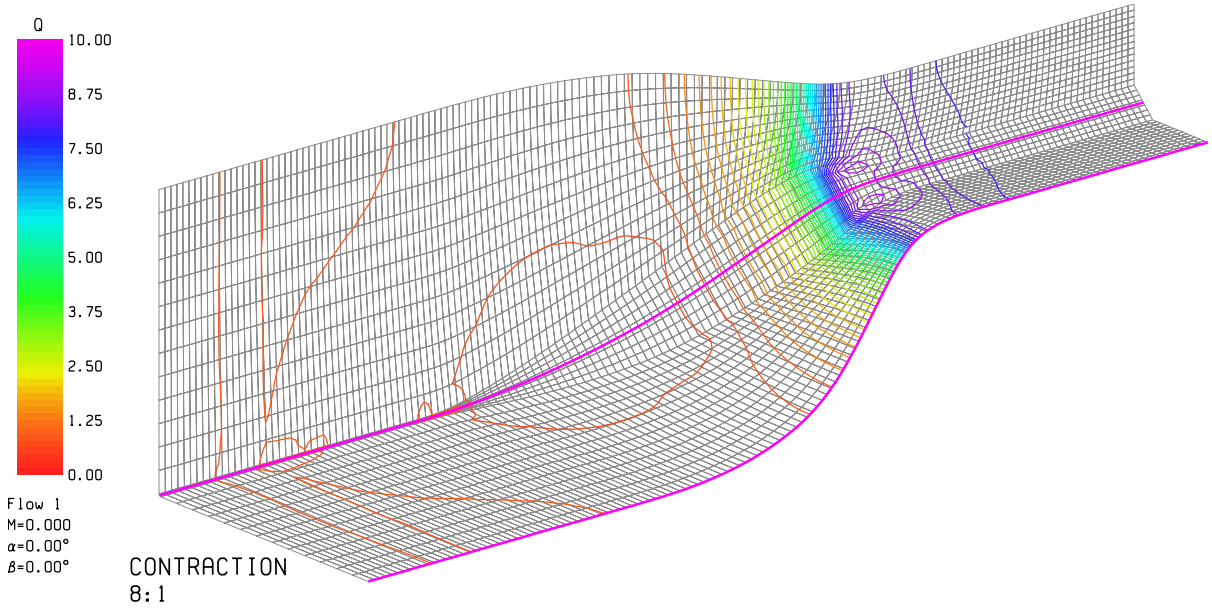

Fig. 5 Surface speed contours on lower quadrant of the contraction, computed with QUADPAN. The section from x = -10 to +2 (ft) is shown, where $x = 0$ represents the start of the test section. The two magenta lines are slices for line plots in Figure 6.

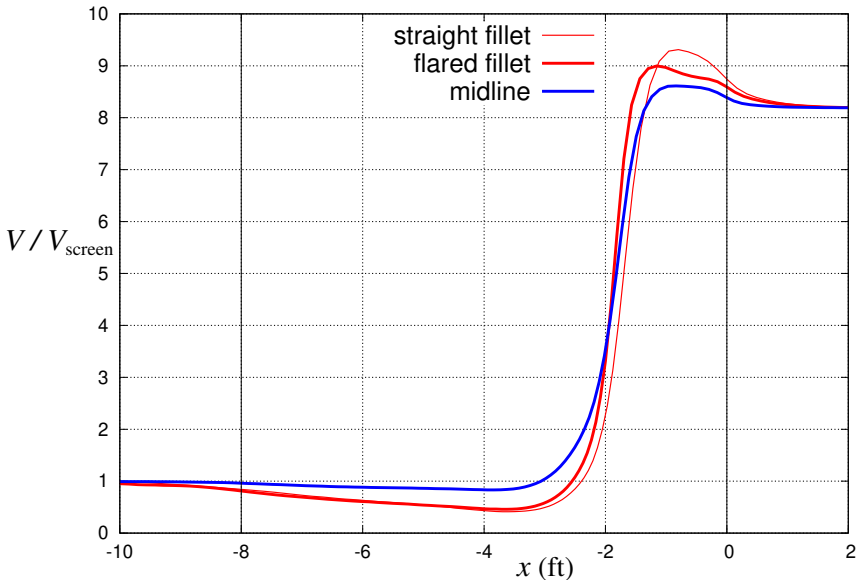

Fig. 6 Surface speed versus x along slice lines shown in Figure 5. Test section begins at $x = 0$.

Table 1 Turbulence-reducing screens specifications

No.	Mesh (per-inch)	Diameter (mm)	Solidity (%)	K [7]
1	14	0.50	48	1.38
2	20	0.23	33	0.64
3	20	0.23	33	0.64
4	20	0.23	33	0.64
5	40	0.20	53	1.84

F. Turbulence screens

Five stainless steel, seamless turbulence-reducing screens are installed just upstream of the contraction. Following the recommendations of [7], the screens have varying mesh size, as indicated in table 1. It is worth noting that the last Screen no. 5 has a solidity of 53% which violates one of the key guidelines of turbulence screen selection — that the solidity remain below 50% [1, 7]. The use of this screen was an error in the screen purchasing and not in the original tunnel design, which called for a screen with lower solidity. As will be discussed in Section IV.B, this screen may be responsible for the higher turbulence levels observed at higher test section speeds. This screen will be replaced in the near future with one having a lower solidity, but for the time being, it has been left in place until its impact on the flow can be fully assessed.

G. Test section

The test section is designed to be reconfigurable to handle many different types of tests and instrumentation. It is comprised of three interchangeable modules, each measuring 1.2 x 1.2 meters in cross section and 1.4 meters in length. All four sides have removable panels so that a variety of wall, floor and ceiling systems can be easily installed, including clear panels for optical access or structural panels, from which to mount models from the side, top or bottom of the working section. Mounting rails for cameras, lasers, etc, run along the top of each module. Gull-wing doors on the two side walls facilitate easy access to the test section for model installation and adjustment. A removable frame in between each of the test section modules can be used to mount additional screens, or instrumentation. The test section has corner fillets that are matched with those of the contraction and decrease in size as one moves downstream to account for boundary layer growth in the working section.

One of the test section modules is fitted with an Aerolab Model Positioning System (MPS) and sting assembly which provides a computer-controlled Pitch & Yaw system for aerodynamic model testing.

Fig. 7 Photograph of test section, looking from the downstream end. The entire test section is enclosed in "the White House" which can be used as a Biosafety-II room during animal flight testing. One of the adjustable pressure-equalization slots is visible at the far left side of the photo.

H. Heat exchanger and instrumentation

The heat exchanger, located upstream of Corner 3, serves to control the air temperature in the test section. The cooling liquid is a water-glycol mixture connected to a dedicated chiller located outside the laboratory building.

Several sensors are used to monitor and control the tunnel operation. Temperature thermistors are located in the large "settling chamber" end of the contraction, and immediately upstream and downstream of the heat exchanger. The temperature of the coolant is also monitored at the entrance and the exit of the heat exchanger. A high accuracy pressure transducer (Mensor CPT6100) measures the differential pressure between static rings located at the entrance and exit of the contraction, and a Pitot tube is mounted in the test section to serve as a double-check against calibration errors

associated with the static ring measurement of the freestream velocity. Sensors for ambient humidity and absolute pressure are located in the large portion of the contraction.

I. Considerations for engineering and animal flight experiments

As mentioned in the introduction, the wind tunnel will be used for two key research objectives — (i) animal flight research and (ii) engineering research and model testing. Several features of the facility design make these two distinct applications feasible and convenient:

- The test section modules are separated by removable frames, allowing wire-mesh screens to be placed immediately upstream of module 2 and downstream of module 3 for animal flight testing. Although this raises the turbulence level in the test section by a moderate amount, it creates a flight area approximately 2.5 meters long in which birds or bats can fly, but from which they cannot "escape" into the rest of the wind tunnel volume (i.e. into the turning vanes and the fan). The screens are easily removed after animal testing so that the turbulence level is again at its minimal level.
- The test section is enclosed in "the White House" — a biosafety enclosure that is held at negative pressure, drawing air in through an air filter in the ceiling and exhausting the air through HEPA-filters at the ground level. This configuration ensures that the testing space is isolated from the rest of the laboratory space so that (i) any animal that accidentally escapes the test section will not be lost to the rest of the lab, and (ii) that any infectious agent that might be introduced by the animals during testing is contained within the testing volume and is filtered from the air before it can pose a risk to un-vaccinated personnel in the larger laboratory space outside. The white house also provides optical isolation for laser light being used in the test section for PIV.
- The cooling system is sized to maintain approximately ambient temperature conditions, even at high test section speeds. This control is critical for engineering testing at high speeds. However, the cooling system can also be used to achieve a range of temperatures at low speeds which are more appropriate for animal flight experiments. By running the cooling system at its highest capacity while still operating the tunnel at low speeds, the ambient temperature of the test section can be lowered to as low as 50°F. Conversely, if one runs the tunnel empty for a few minutes at the highest speed without any cooling, the air temperature inside rises (quickly), after which low-speed animal flight experiments can be performed at the elevated temperatures.

IV. Wind tunnel performance

The mechanical design and fabrication of the facility was completed by Aerolab (Jessup, MD). Installation was largely complete by May 2019 after which time several experiments were conducted to assess the tunnel performance. A hot wire anemometer was mounted on a two-axis traversing mechanism positioned 140 cm from the test section entrance. The hot wire was calibrated against a Pitot tube and traversed over the central portion of the test section. It was not possible to traverse the hot wire over the test section at speeds higher than 20 m/s due to vibrations in the supporting sting which was not robust enough to support the hot wire probe and to traverse at freestream velocities. This measurement will be left for a later date. To assess the turbulence levels at higher test section velocities, the hot wire probe was attached to a rigid post at the center of the test section and the turbulence level was measured over the entire velocity range of the wind tunnel from 2 to 45 m/s.

A separate experiment was conducted to assess flow angularity. For this, a custom-designed angularity probe was attached to the traversing system and traversed over the central portion of the test section at several speeds.

A. Flow Uniformity and angularity

Initial measurements of flow uniformity were performed using a hot wire anemometer which was traversed over entire test section. However, we do not present those results here due to some experimental inconsistencies. Unfortunately, due to the COVID-19 pandemic, we were not able to repeat those measurements prior to the submission deadline for this paper. These measurements will be repeated, along with flow angularity measurements and the results will be reported in a subsequent publication.

B. Turbulence levels

At each y–z (spanwise-vertical) location, 30 seconds of hot wire data was acquired using a 24 bit ADC at 17kHz (National Instruments 9234) and converted to velocity using a fifth-order polynomial calibration. The raw hot wire voltage was also recorded after first high-pass filtering with a 4Hz analog Butterworth filter and amplifying by an

additional 20dB (Kron-hite 3342). In post-processing the average (DC) voltage was added back to the re-scaled high-pass filtered voltage and the composite signal converted to a velocity, yielding a high-resolution high-pass filtered velocity signal. Both signals were then scaled by the mean velocity and turbulence levels were computed from the variance of the signals. Spectra of the freestream turbulence were calculated using the Welch estimate with 50% buffer overlap and a Hanning window.

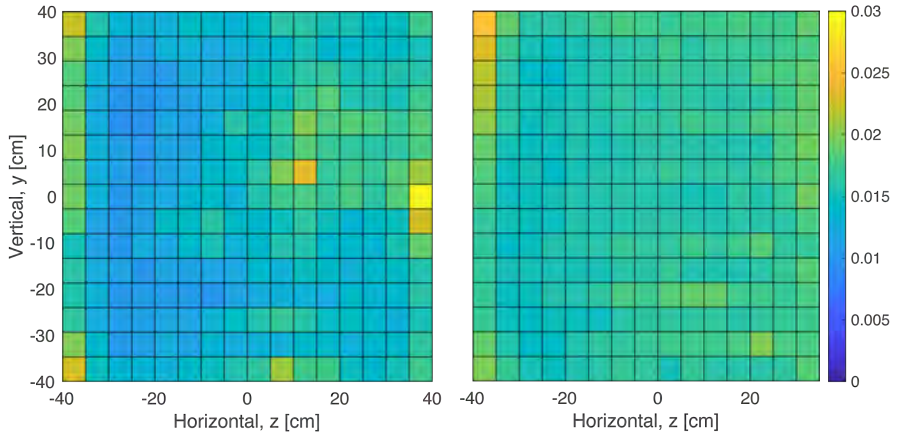

Fig. 8 Spatial distribution of turbulence (u/U in %), measured using a hot wire anemometer over the central portion of the test section at two speeds: $U = 4$ and 7 m/s.

The spatial distribution of turbulence is shown in figure 8 for freestream velocities of 4 and 7 m/s. The low level of turbulence is observed throughout the test section with a few anomalous locations which may be due to measurement glitches, but do not seem to be consistent over the range of velocities tested. The right side of the test section shows a slight increase in turbulence level which may be associated with presence of a stationary Pitot tube upstream of that location. Overall, the turbulence level is very good with no position recording a turbulence level higher that 0.03% (4Hz – 8.5 kHz bandwidth). Low-frequency fluctuations in the local velocity increased the turbulence level to 0.05% over a 0.03Hz - 8.5kHz bandwidth.

A sample power spectrum from the center line of the test section at a freestream velocity of 12m/s is shown in figure 9. At this particular location and speed the overall turbulence level (the integral over all frequencies) is very low — 0.046% for the 0.03–8500 Hz bandwidth and 0.024% for the 4–8500 Hz bandwidth. As expected the dominant contribution to the turbulence comes at low frequencies, but there is a slight “bulge" in the 100–200 Hz range, and a few discrete spikes which can be related to the fan rotation frequency and the blade passage frequencies associated with this speed. There is no contribution to the overall turbulence level from frequencies above 4 kHz. Note that there is

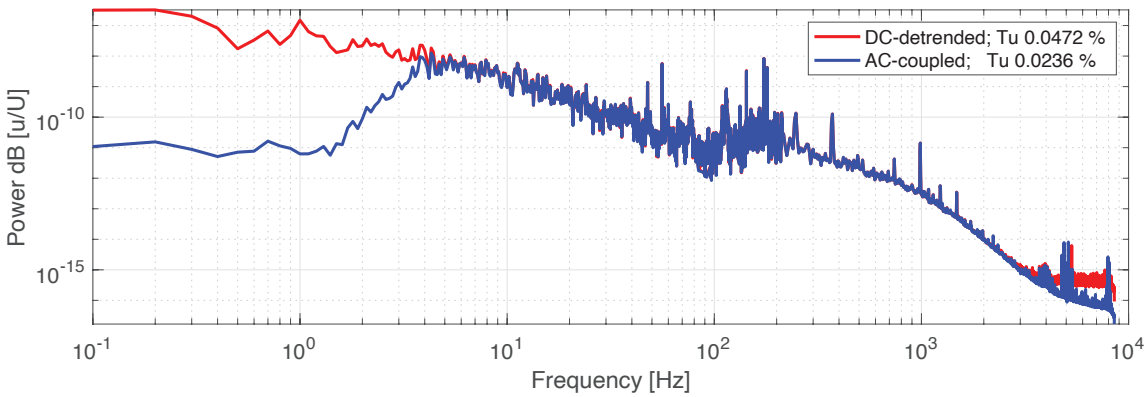

Fig. 9 Sample turbulence spectrum in the center of the test section, $(y, z) = (0, 0)$. Freestream velocity, $U = 12$ m/s, Red: 0.03 Hz– 8.5 kHz bandwidth, Blue: 4.0 Hz – 8.5 kHz bandwidth.

no difference between the DC and AC-coupled signals, except for the absence of energy below 4 Hz in the high-pass filtered signal (not surprising) and the slightly lower noise floor in the AC-coupled signal, which was amplified before digitizing and hence able to resolve velocity fluctuations with even higher resolution. Nevertheless, the overall very low turbulence level of the facility is quite remarkable.

V. Conclusions and outlook

Although the facility is still new and we are still learning about its performance over the full range of operating speeds, the initial indications are that the innovative aspects of the design — the expanding corners, the screened turning vane in Corner 4 and the short contraction — have performed as expected, and that the flow quality is excellent. More assessments are still needed, particularly detailed mean flow measurements of flow uniformity, angularity and temperature stability, as well as extensive measurements at higher freestream velocities more common for engineering model testing. Due to the COVID-19 pandemic, these measurements could not be completed in time for this paper's publication deadline. Nevertheless, the tentative conclusions are that this is a very appealing approach for the design of efficient, cost-effective and compact low-speed wind tunnels.

Acknowledgments

The new wind tunnel was funded by a Major Research Infrastructure (MRI) grant from the National Science Foundation, with matching funds from Brown University. Brown University also contributed additional resources towards the preparation of the site prior to the wind tunnel installation. Quincy McKeon, Anna Seto, Katherine Pisani, Hunter Ray, Ben Lyons, Paul Waltz, Paul Vasilescu, and Baruch Weiner contributed enormously to the many aspects of the design, fabrication, installation and qualification of the facility, and their efforts are most gratefully acknowledged.

References

[1] Bradshaw, P., and Pankhurst, R. C., "The design of low-speed wind tunnels," *Progress in Aerospace Sciences*, Vol. 5, 1964, pp. 1–69.

[2] Lindgren, B., and Johannson, A. V., "Evaluation of a new wind tunnel with expanding corners," *Experiments in Fluids*, Vol. 36, 2004, pp. 197–203. https://doi.org/10.1007/s00348-003-0705-y.

[3] Lindgren, B., Osterlund, J., and Johannson, A. V., "Measurement and Calculation of Guide Vane Performance in Expanding Bends for Wind-Tunnels," *Experiments in Fluids*, Vol. 24, 1998, pp. 265–272.

[4] Drela, M., Huang, A., and Darmofal, D., "Screened Expanding Turning Vane Concept," *Experiments in Fluids*, Vol. 61, 2020. https://doi.org/10.1007/s00348-020-2910-3, URL https://dspace.mit.edu/handle/1721.1/123882.

[5] Giles, M., and Drela, M., "Two-Dimensional Transonic Aerodynamic Design Method," *AIAA Journal*, Vol. 25, No. 9, 1987, pp. 1199–1206.

[6] Youngren, H., Bouchard, E., Coopersmith, R., and Miranda, L., "Comparison of Panel Method Formulations and its Influence on the Development of QUADPAN, an Advanced Low Order Method," AIAA-1983-1827, 1988.

[7] Groth, J., and Johansson, A. V., "Turbulence reduction by screens," *Journal of Fluid Mechanics*, Vol. 197, 1988, pp. 139–155.